BIOCHEMISTRY
including biophysical chemistry & molecular biology

Article

pubs.acs.org/biochemistry

Mapping Molecular Flexibility of Proteins with Site-Directed Spin Labeling: A Case Study of Myoglobin

Carlos J. López, Shirley Oga, and Wayne L. Hubbell*

Department of Chemistry and Biochemistry, Jules Stein Eye Institute, University of California, Los Angeles, California 90095-7008, United States

Supporting Information

ABSTRACT: Site-directed spin labeling (SDSL) has potential for mapping protein flexibility under physiological conditions. The purpose of the present study was to explore this potential using 38 singly spin-labeled mutants of myoglobin distributed throughout the sequence. Correlation of the EPR spectra with protein structure provides new evidence that the site-dependent variation in line shape, and hence motion of the spin label, is due largely to differences in mobility of the helical backbone in the ns time range. Fluctuations between conformational substates, typically in the μs−ms time range, are slow on the EPR time scale, and the spectra provide a snapshot of conformational equilibria frozen in time as revealed by multiple components in the spectra. A recent study showed that osmolyte perturbation can positively identify conformational exchange as the origin of multicomponent spectra (López et al. (2009), *Protein Sci. 18*, 1637). In the present study, this new strategy is employed in combination with line shape analysis and pulsed-EPR interspin distance measurements to investigate the conformation and flexibility of myoglobin in three folded and partially folded states. The regions identified to be in conformational exchange in the three forms agree remarkably well with those assigned by NMR, but the faster time scale of EPR allows characterization of localized states not detected in NMR. Collectively, the results suggest that SDSL-EPR and osmolyte perturbation provide a facile means for mapping the amplitude of fast backbone fluctuations and for detecting sequences in slow conformational exchange in folded and partially folded protein sequences.

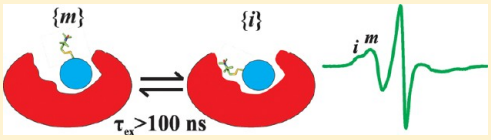

Proteins in solution exhibit a hierarchical flexibility that encompasses a range of time and length scales, and this flexibility may be intimately related to function. Conformational flexibility corresponds to interconversion (exchange) between discrete conformational substates that have lifetimes typically on the μs to ms time scale.[1−3] Structural changes corresponding to transitions between substates range from simple rigid body movements of helices to large scale rearrangements of entire domains. The existence of conformational substates in equilibrium can account for promiscuity in protein−protein and protein−ligand interactions,[4−8] and provides a framework for describing molecular switching in terms of shifting equilibrium populations of substates in response to changes in the energy landscape triggered by external signals.[7]

Within each conformational substate, there is a large number of "statistical" substates[2] each with different dihedral angles in the backbone and side chains. The lifetime of these substates is in the ps−ns range, and transitions between them correspond to fast backbone and side chain fluctuations. Backbone motions on this time scale can range from small amplitude oscillations about an average regular structure to large amplitude motions corresponding to dynamic disorder in a sequence. Intrinsically disordered sequences apparently play a role in protein−protein interactions and ligand binding,[9] as well as in providing hinge-regions that allow transitions between conformational substates.[3]

Thus, to understand molecular mechanisms underlying protein function, it is necessary to have experimental strategies that are capable of detecting the existence of conformational substates at equilibrium, measuring the exchange rates between them, and identifying dynamically disordered sequences within a substate. NMR spectroscopy has been particularly effective in providing atomic level information on dynamics for proteins in solution.[10,11] However solution NMR is challenged for application to membrane-bound proteins in their native lipid environment under physiological conditions and for studying nonequilibrium states that evolve in time. Our laboratory is interested in the role of protein flexibility in G-protein coupled signal transduction, a system that involves precisely these situations. To enable facile study of such systems, we are exploring strategies based on site-directed spin labeling (SDSL) and EPR spectroscopy, which has high sensitivity, a time scale favorable for measuring protein dynamics, and has no limitations as to the size or complexity of the systems that can be studied under native-like conditions.

In SDSL, a paramagnetic side chain is introduced site-specifically. The most commonly used nitroxide side chain is R1 (see inset in Figure 1), although many others have been developed.[12−15] The EPR spectrum of an R1-labeled protein reflects the overall motion of the nitroxide in the 0.1−100 ns time scale; this is the intrinsic time window through which the dynamics of R1 is viewed via an X-band EPR spectrum. Thus, backbone fluctuations that occur in this time range must

Received: May 1, 2012
Revised: July 9, 2012
Published: July 18, 2012

dx.doi.org/10.1021/bi3005686 | *Biochemistry* 2012, 51, 6568−6583

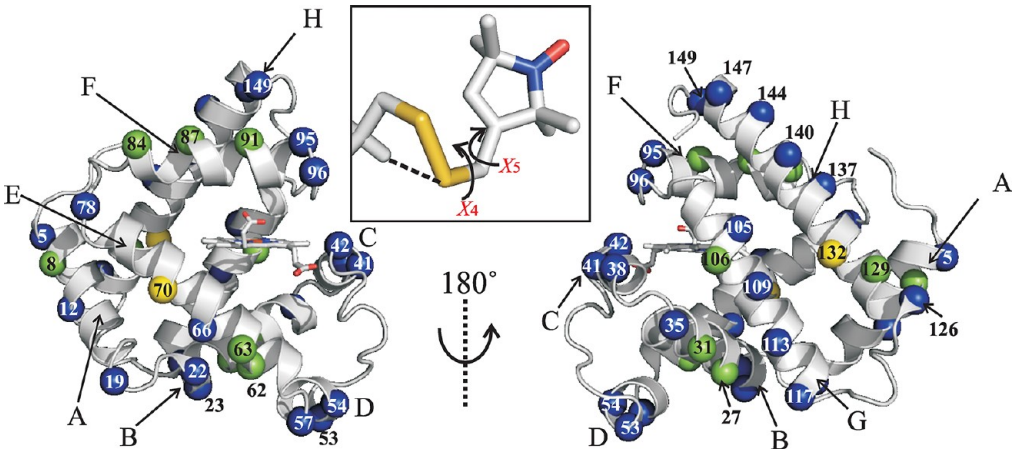

Figure 1. Ribbon diagram of myoglobin (PDB code 2MBW)[25] showing the positions where the R1 side chain was introduced. The spheres at the Cα indicate the sites where the EPR spectra reflect single (blue and yellow) and multiple (green) components (see text). The yellow spheres indicate sites where the spectra reflect a single component, but of S > 0.5. Inset: Stick representation of the R1 side chain showing the intraresidue Sδ-Hα interaction[14,43,49] that restricts the internal motion of all dihedral angles except the last two (X_4/X_5 model).[14,48,49]

contribute directly to the EPR spectral line shape.[16,17] Indeed, the capability of SDSL to identify large amplitude ns motions of the backbone in unstable helical structures has been well documented.[17] Subtle variations in R1 motion between sites in stable helices have also been attributed to differences in local backbone fluctuations;[16] however, recent theoretical studies imply that local interactions and rotamer exchange of R1 may play an important role.[18] The present study provides new data that may be taken as support for a dominant role of backbone fluctuations.

Unlike that for backbone fluctuations, the characteristic time scale of exchange between conformational substates in equilibrium is too slow to produce magnetic relaxation; thus, no information on exchange dynamics is contained in the spectrum. However, the existence of multiple conformational substates can be directly revealed by multiple components in the spectrum,[19−21] thereby providing a snapshot of conformational equilibria frozen in time, with no averaging effects. EPR spectra of spin-labeled proteins often contain multiple components, but only a subset of these represents conformational exchange because multicomponent spectra can also arise from multiple rotamers of R1 at a given site, wherein each rotamer experiences a unique environment.[22,23] Several experimental strategies have recently been developed to distinguish conformational from rotameric equilibria as the origins of multicomponent spectra in SDSL, namely, osmolye perturbation EPR,[19] high pressure EPR,[21] pulsed saturation recovery (SR) EPR,[20] and pulsed electron−electron double resonance (ELDOR).[15] Among these strategies, the SR and ELDOR methods can measure exchange rates on the functionally important μs time scale.

In principle then, SDSL-EPR has the potential to provide a sequence-specific map of backbone fluctuations in the ps−ns range and of regions in slow (μs−ms) conformational exchange. The purpose of this article is to present the results of the first comprehensive study aimed at evaluating this potential using myoglobin as a model system. Spectral line shape analysis is used to identify dynamically disordered sequences and to elucidate structural features underlying the variation of R1 motion in ordered helices, while osmolyte perturbation is employed to identify site-specific conformational equilibria in various states of the protein.

Myoglobin is an ideal model system, particularly for exploring conformational equilibria, because conditions have been established for which folded and partially folded states are populated under equilibrium conditions suitable for biophysical characterization. The states are (1) native holo (N_{Holo}) containing the heme ligand; (2) native apo (N_{Apo}); (3) a locally unfolded intermediate[24] (I); (4) the molten globule intermediate (I_{MG}); and (5) the acid unfolded state (U_{Acid}). High resolution crystal structures are available for the holo form,[25,26] while solution NMR[24,27−34] and CD spectroscopy,[35] along with small-angle X-ray scattering,[36] and mass spectrometry[37] have provided a wealth of information on the structure and dynamics of the protein in solution for each of the states.

In the work reported here, R1 was placed, one at a time, at 38 individual solvent-exposed sites throughout myoglobin, and the EPR spectra were recorded in three of the aforementioned states (i.e., N_{Holo}, N_{Apo}, and I_{MG}). In addition, distance measurements between R1 pairs were determined using double electron−electron resonance (DEER) spectroscopy to provide structural insights into the changes that follow the $N_{Holo} \rightarrow N_{Apo} \rightarrow I_{MG}$ transitions.

Analysis of R1 spectra at sites throughout the solvent-exposed surface of N_{Holo} reveals that site-to-site variation of R1 motion in helices is correlated with the fraction of buried surface area of the helical segment containing the spin label; this is consistent with a model in which the variation of R1 motion results from backbone fluctuations that are modulated by local interactions. A map of conformational flexibility in the various states, deduced from osmolyte perturbation, is in excellent agreement with results from NMR, to the extent that they can be compared. Importantly, the data provide additional insight into the conformational properties of sequences for which direct information was not accessible by other methods.

EXPERIMENTAL PROCEDURES

Construction, Expression, and Purification of Myoglobin Mutants. The plasmid pET17b (Novagen, Madison WI) carrying the WT gene of sperm whale myoglobin was kindly provided by Steven Boxer (Stanford University). The individual cysteine substitutions were introduced by using the QuikChange Method (Stratagene, La Jolla, Ca). All mutations were confirmed by DNA sequencing. Mutant plasmids were

dx.doi.org/10.1021/bi3005686 | Biochemistry 2012, 51, 6568−6583

transformed into the expression cells *E. coli* BL21(DE3), and the protein was expressed and purified from inclusion bodies as previously described[38] with some modifications. Briefly, the washed inclusion body pellets were resolubilized in a solution containing 40%−50% acetonitrile/0.1% trifluoroacetic acid followed by sonication. The resolubilized inclusion bodies were subjected to centrifugation at 15,000 rpm for 15 min to remove any insoluble material. The protein was purified by reverse-phase HPLC using a linear gradient (20−100%) of an acetonitrile solution containing 0.1% trifluoroacetic acid as a mobile phase. Following HPLC purification, the protein fractions containing myoglobin (as judged by SDS−PAGE) were lyophilized and stored at 4 °C until needed.

Resolubilization of Lyophilized Protein, Size-Exclusion Chromatography, and Spin-Labeling of Myoglobin Mutants. The lyophilized protein was resuspended in a freshly made resolubilization solution (10 mM sodium acetate, 6 M urea, and 5 mM DTT at pH 6.1). The protein solution was allowed to equilibrate at 4 °C for at least 30 min. *In vitro* refolding of myoglobin was achieved by a rapid 10-fold dilution of the urea-denatured protein into the refolding buffer (10 mM sodium acetate and 5 mM DTT at pH 6.1). The protein concentration during refolding was maintained at or below 1 mg/mL to minimize aggregation. For some mutants, higher yields from *in vitro* refolding were achieved by overnight dialysis of the urea-denatured protein into the refolding buffer instead of rapid-dilution (Figure S1, Supporting Information). DTT was removed using a Hi-Trap desalting column (GE Healthcare) and the eluted protein was immediately incubated with 10-fold molar excess of 1-oxyl-3-methanesulfonylthiomethy-2,5-dihydro-2,2,5,5 tetramethyl-1*H*-pyrrole (MTSL)[14] reagent and allowed to react overnight at 4 °C. Excess spin label was removed, and the buffer was exchanged with gel filtration buffer (10 mM sodium acetate and 100 mM NaCl at pH 6.1) on the Hi-Trap desalting column. To separate the correctly folded monomeric species from any soluble misfolded aggregates, the spin-labeled protein was injected into a Superdex 75 column (GE Healthcare) equilibrated with gel filtration buffer. The misfolded and correctly folded fractions eluted at V_e of ∼7.6 mL and ∼12.6 mL (±0.1 mL), respectively (Figure S1, Supporting Information). The monomeric protein at this point was >95% pure (as judged by SDS−PAGE). For EPR studies of myoglobin in the N_{Apo} state, the buffer was exchanged with 10 mM sodium acetate at pH 6.1, and the proteins were concentrated to ∼400 μM with Amicon ultra concentrator (10 kDa MWCO: Millipore). Protein concentrations were determined by the absorbance at 280 nm using an extinction coefficient of 15,400 M^{-1} cm^{-1}.

For EPR studies of myoglobin in the N_{Holo} state, the apoprotein at pH 6.1 was incubated with a 1.2-fold molar excess of bovine hemin (Sigma) dissolved in 10 mM NaOH (concentration of stock hemin solution was 10 mM), and the solution was incubated overnight at 4 °C. Excess of heme was removed using the Amicon ultra concentrator, and the binding of heme was assessed via a UV−vis scan (Figure S4, Supporting Information). The holo-protein reconstituted in this manner auto-oxidizes into the aquomet form (Fe^{3+}−H_2O) as judged by the absorption maxima at 409 nm.[39] The aquomet myoglobin samples were concentrated to ∼400 μM as judged by the absorbance at 409 nm using an extinction coefficient of 157,000 $M^{-1}cm^{-1}$.

For studies of myoglobin in the I_{MG} state, the buffer solution was exchanged by repeated washes (5 × 15 mL each) with buffer containing 10 mM sodium acetate at pH 4.1 using the amicon concentrator. To populate the U_{Acid} state (see Supporting Information), the protein solution was exchange with a solution consisting of 10 mM acetic acid/HCl at pH 2.3.

EPR Spectroscopy. The continuous wave (CW) EPR spectra of spin-labeled myoglobin mutants were recorded in a Bruker ELEXSYS 580 fitted with a high sensitivity resonator at 298 K using an incident microwave power of 20 mW and a modulation amplitude of 1 G. Samples of at least 6 μL were loaded in sealed capillary tubes (0.6 ID × 0.84 OD; VitroCom, Inc., NJ). Spectra were recorded at X-band frequency with a scan width of 100 G. Solution spectra were recorded either in 30% w/w sucrose or 25% w/w Ficoll 70 solutions with a final protein concentration of 200−400 μM. To obtain the EPR spectra of protein immobilized on the CNBr solid support, the protein was coupled to a cyanogen bromide activated Sepharose (GE Healthcare) as previously described.[19] Fifty microliters of the gel slurry containing spin-labeled myoglobin was loaded into a quartz capillary tube (1.5 ID × 1.8 OD; VitroCom Inc., NJ).

Root mean square differences (rmsd) of the EPR spectra were computed after baseline correction, alignment, and normalization using software developed in LabView by Christian Altenbach.

DEER Spectroscopy. The four-pulse DEER experiment for the double spin-labeled myoglobin mutants was conducted according to published procedures.[40] The protein concentration during the DEER experiments were maintained at or below 200 μM. Twenty microliters of myoglobin samples at the appropriate buffer conditions containing 20% v/v glycerol as cryoprotectant were loaded into a quartz capillary tube (1.5 ID × 1.8 OD; VitroCom Inc., NJ) and then flash-frozen in liquid nitrogen. The DEER measurements were performed at 80 K on the Bruker ELEXSYS 580 fitted with a 2-mm split ring resonator. Distance distributions were obtained from the raw dipolar evolution time data using the DEER Analysis 2009 program (available at http://www.epr.ethz.ch/software/index) and by fitting the background-subtracted dipolar evolution data using Tikhonov regularization.[41]

Fraction of Surface-Buried. The fraction of solvent-accessible areas for each side chain ($f_{acc,R}$) was calculated with Getarea[42] using the high-resolution structure of myoglobin (PDB ID: 2mbw) and a probe radius of 1.4 Å. The fraction of solvent-inaccessible (buried) area per side chain was computed as $f_{buried,R} = 1 - f_{acc,R}$. The fraction of surface buried for a helical segment bearing the nitroxide was then computed as

$$f_{\text{buried}=1/n} \sum_{i=1}^{n} f_{\text{buried},R_i}$$

where the sum extends over side chains i in a segment of $n = 6$ or $n = 9$ residues. The short windows (6 residues) were used for cases in which the nitroxide was introduced near a helix terminus and for short helices (helices C and D), whereas the 9-residue (from $i - 4$ to $i + 4$) window was used for R1 in the center of helices.

RESULTS

Characterization of the Mutants. For this study, 41 single cysteine substitution mutants at solvent exposed sites of myoglobin were engineered throughout α-helices A to H and three of the interhelical turns (i.e., the A/B, E/F, and G/H) (Figure 1), and subsequently spin labeled with the R1 side

chain. Some of the mutants formed soluble oligomeric species in addition to the monomer following isolation and refolding of the N_{Apo} form, presumably due to misfolding (Figure S1, Supporting Information). In such cases, it was found to be essential to remove the oligomeric species which contributed to the EPR spectra of the spin-labeled mutants. In three cases (R118C, A127C, and K133C) oligomerization was essentially complete, and these mutants were not investigated further. Thus, 38 of the mutants were employed in the following experiments.

Previous crystallographic studies have shown that introduction of the R1 at surface sites causes little structural perturbation in soluble[14,22,23,43] and membrane[44] proteins. Indeed, for the purified monomeric apomyoglobin, substitution of R1 at surface sites caused little change in the secondary structure for the cases investigated as judged by Far UV CD spectroscopy (Figure S3, Supporting Information). In addition, mutations of the surface residues did not impair heme binding to the apo protein (Figure S4, Supporting Information), as expected.[45]

R1 Motion in the Helices of N_{Holo}. The EPR spectrum of a spin-labeled protein encodes information on the overall motion of the nitroxide ring on the nanosecond time scale with contributions from: (1) the internal motion of the R1 side chain, which can be modulated by interactions of the nitroxide with the environment, (2) local backbone fluctuations, and (3) rotational diffusion of the protein.

The contribution from the rotational diffusion of the protein can be minimized by increasing the effective viscosity of the protein solution[46] or by immobilizing the protein on a solid support.[19] In the present study, 25% w/w Ficoll 70 is employed as a viscogen to effectively eliminate the effects of overall rotational diffusion. Ficoll 70 at this concentration has no effect on the internal motions of the R1 side chain,[19,47] does not affect the secondary structure or the stability of the protein in the N_{Apo} state,[19] and has only minor effects on the stability of the I_{MG} globule state (Figure S3 and Table S1, Supporting Information), suggesting that crowding effects are minimal. Thus, the EPR spectra recorded in solutions of Ficoll 70 at 25% w/w are taken to primarily reflect the R1 internal motion and any contributions from ns backbone dynamics.

At noninteracting solvent exposed sites in helices and loops, the purely internal motion of R1 is believed to give rise to a single-component EPR spectral line shape reflecting an anisotropic motion that can be described by an order parameter (S) ≈ 0.5 and a rate (τ^{-1}) of approximately 0.5 ns^{-1}, where τ is the effective correlation time.[13,17] An operational definition of a "noninteracting" site is one at which the R1 side chain makes no contacts with neighboring residues and where $S \leq 0.5$; increased ordering beyond 0.5 is believed to arise from interactions of the nitroxide with the environment.[43,48,49] The structural basis of the internal motion of R1 has been elucidated through high-resolution structures of spin-labeled proteins,[14,22,23,43] variation of side chain structure,[12,13] mutational analysis,[14,46] and quantum mechanical calculations.[50] An outcome from these studies is a model of internal motion of the R1 side chain known as the X_4/X_5 model (see inset in Figure 1).[13,14] Within the context of this model, the internal motions of the side chain for noninteracting surface sites should be independent of the sequence position, and hence, the site-to-site variations in S and τ for such sites are a reflection of differences in the local backbone fluctuations.[16,17]

The present study examines the position-dependent variation of R1 motion in the helices of N_{Holo} myoglobin for which NMR relaxation[29] and hydrogen exchange[31] studies reveal stable secondary structures. Remarkably, 26 of the 38 sites studied throughout N_{Holo} meet the criteria for noninteracting surface sites. The sites are identified in Figure 1 (blue spheres), and the EPR spectra for R1 at representative sites are shown in Figure 2; the complete data set is provided in Figure S5 (Supporting Information). The resolved spectral features in the spectra of sites 66R1, 95R1, and 113R1 are the parallel (||) and perpendicular (⊥) hyperfine components (Figure 2) characteristic of an anisotropic motion of the nitroxide with $S \geq 0.3$.[17]

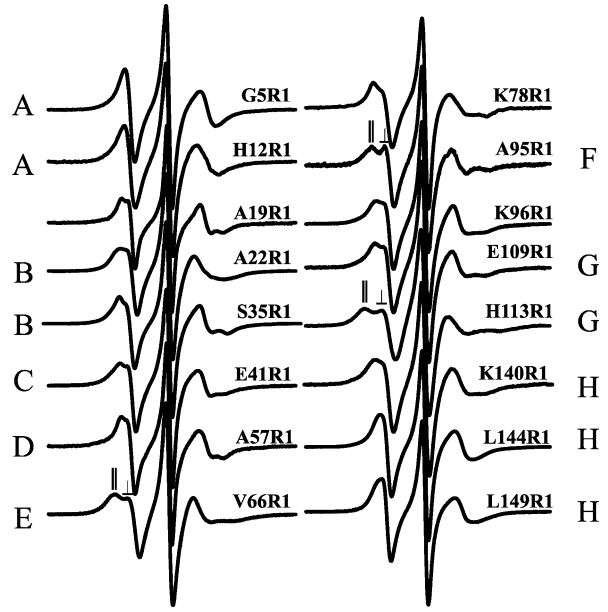

Figure 2. Representative EPR spectra in N_{Holo} that reflect a single dynamic state. The helix in which each R1 side chain is located is indicated. The symbols ⊥ and || identify the well-resolved hyperfine components.[17]

Although the spectral line shapes in Figure 2 all reflect anisotropic motion, there is a variation in detail from site-to-site attributable to differences in amplitude and/or rate of motion on the ns time scale. The spectral differences can be measured by an empirical "scaled mobility" parameter (M_s) determined directly from the spectral central line width and proportional to τ^{-1} for weakly anisotropic motion.[17] Alternatively, numerical values for both S and τ^{-1} can be determined by fitting the entire spectrum to the MOMD model of Freed and co-workers.[51] If the variations in S and/or M_s and τ^{-1} are due to local backbone fluctuations in a helical segment, it is intuitively reasonable to expect a correlation of these parameters with the number of atomic contacts made by the helical segment containing R1; as the number of contacts increases, one would expect S to increase and the rate of motion, measured by M_s or τ^{-1}, to decrease. This is indeed the case for the empirical parameter M_s as shown in Figure 3A, where the number of contacts is conveniently measured by the fraction of buried surface area (f_{buried}) for a segment of 6−9 residues around the R1 site (see Experimental Procedures).

Fits of the spectra to the MOMD model were done for 13 representative sites from the set of 28, and a plot of both S and τ^{-1} determined from the fits versus f_{buried} are given in Figure 3B (the fits and parameters are given in Figure S6 and Table S2,

dx.doi.org/10.1021/bi3005686 | Biochemistry 2012, 51, 6568−6583

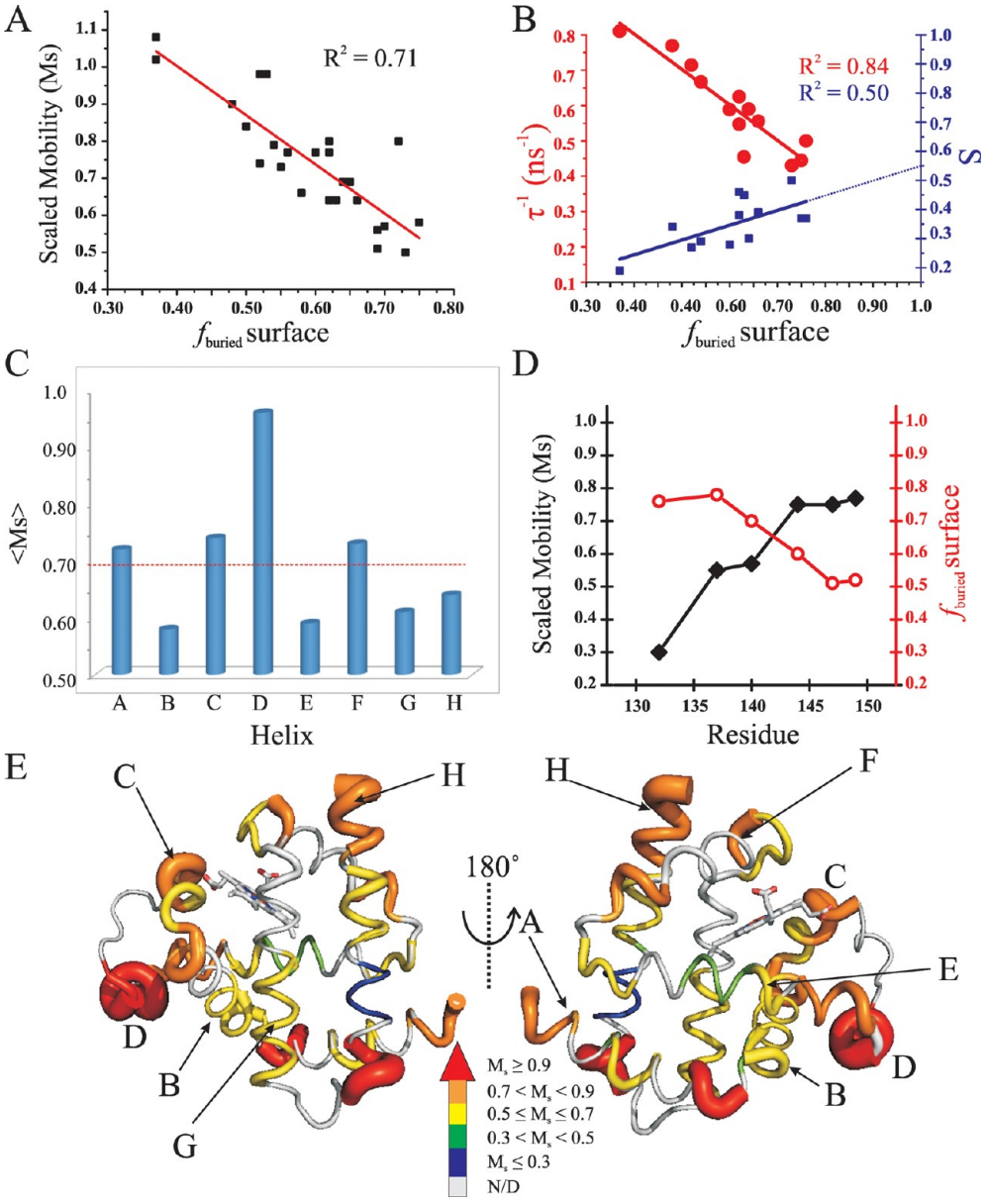

Figure 3. Mapping fast backbone motion in myoglobin with SDSL. (A) Correlation of scaled mobility (M_s) with a fraction of the surface buried (see Experimental Procedures). (B) Correlation between rate (τ^{-1}) and order of motion (S) of R1 with a local fraction of the surface buried. (C) Mean M_s value per helical segment. The dashed red line indicates the overall average value. (D) M_s values and local fraction of the surface buried for residues within the H-helix. (E) Cartoon representation of myoglobin indicating the mobility of the nitroxide as judged by the M_s values. The width and color of the backbone are proportional to M_s (N/D: not determined).

Supporting Information, respectively). As for M_s, the rate of motion measured by τ^{-1} is inversely correlated with f_{buried}, while S increases with increasing f_{buried}. Interestingly, extrapolation of S to the hypothetical state of $f_{buried} = 1$ yields $S = 0.55 \pm 0.08$, which is close to the order parameter observed at sites reflecting pure internal motion of R1.[13,16] The correlations shown in Figure 3A and B are consistent with a model in which structural fluctuations of the helix, modulated by packing interactions, play a dominant role in the variation in motion of R1. Figure 3C shows the average value of R1 mobility for each helix as measured by $\langle M_s \rangle$. Within the context of the above model, the data indicate that the short helices C, D, and F are the most flexible in the holomyoglobin molecule on the nanosecond time scale.

M_s for R1 in α-helices could either reflect rigid body motions of an entire helix or local segmental fluctuations.[16] For long helices, where the fraction of surface buried varies along the length of the helix, the site-to-site differences in mobility of the R1 side chain may reflect local segmental motions. Indeed, this appears to be the case in the long helix H sequence. As shown in Figure 3D (see also Figure S7, Supporting Information), a gradient of increasing mobility is observed from residue 132R1 to residue 149R1 at the C-terminus. The fraction of the surface buried along the same sequence (red trace in Figure 3D) shows a decreasing gradient due to the reduction in contact near the C-terminus for which only 25% of the surface interacts with other structural elements.

Results regarding the sequence dependence of M_s are summarized graphically in Figure 3E, which shows relative

dx.doi.org/10.1021/bi3005686 | Biochemistry 2012, 51, 6568−6583

rates of motion on models of N_{Holo} encoded by both color and width of the tube representing the backbone.

Identifying Conformational Flexibility with SDSL. The above analysis of backbone motion employed one-component EPR spectra that reflect a single dynamic mode of R1; such spectra are common for R1 at solvent-exposed sites in rigid helices. However, multiple-component spectra that reflect distinct motions of the nitroxide are often observed for R1 in helices. Generally, one of the components resembles that of a noninteracting surface site such as those shown in Figure 2, while the other reflects immobilization of the nitroxide due to interactions with nearby groups of the protein.[22,23] The immobilized component is resolved as a broad resonance in the outer wings of the spectrum (arrows, Figure 4A). In the slow motional regime of the immobilized state, the spectral line shape is only weakly dependent on mobility, and a spectral component assigned as "immobilized" could in fact consist of multiple unresolved states. For simplicity, spectra with resolved states of relatively high and low mobility will be treated as two-component.

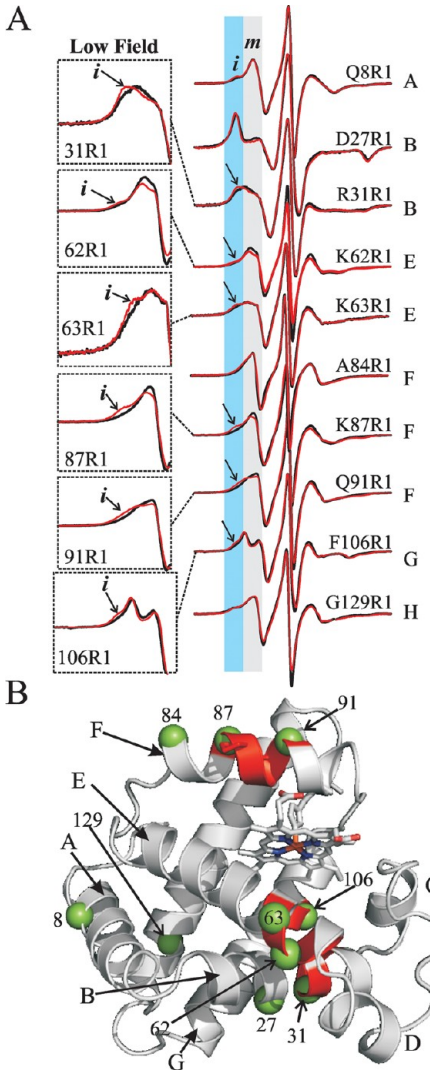

Figure 4. Conformational exchange in N_{Holo}. (A) EPR spectra of R1 at sites with multicomponent spectra in Ficoll 70 (black) and sucrose (red). The light blue and gray shaded areas identify regions where relatively immobile and mobile states of the nitroxide, respectively, contribute to the intensity. The arrows identify an increase in intensity of a more immobile component due to sucrose addition. The low field lines are amplified for clarity. (B) Ribbon diagram of holo myoglobin. The spheres at the Cα indicate the sites where the EPR spectra reflect two components. The regions in conformational exchange as judged by the osmotic shift are colored red.

Two-component spectra can arise from either protein conformational equilibria or the less interesting case of rotameric equilibria of R1.[22,23] One strategy to distinguish these two possibilities is based on osmolyte perturbation.[19] Stabilizing osmolytes such as sucrose shift protein conformational equilibria toward the least solvent-exposed state,[52,53] but have little effect on rotameric equilibria of R1.[19] Thus, if sucrose addition shifts the relative populations in a two-component spectrum, the origin of the two-components is apparently an equilibrium between distinct protein conformational states rather than rotameric equilibria of R1.[19] Because the least solvent-exposed conformation of a protein is the most compact with increased opportunities for interaction of R1, osmotic perturbation generally shifts spectral populations toward more immobilized states.[19,54]

In addition to an osmolyte effect, the 30% w/w sucrose solution used in the present study increases the viscosity and hence reduces the protein rotational diffusion rate. To isolate the pure osmolyte effect, EPR spectra are compared for the protein in sucrose and Ficoll 70, the latter of which increases viscosity, but has no osmolyte effect; the viscosity of 30% w/w sucrose is matched closely by 25% w/w Ficoll 70.[19]

Conformational Flexibility in N_{Holo}. To map sites of conformational flexibility in the N_{Holo} state, all spectra of R1 having two components were compared in Ficoll and sucrose solutions, and the results are shown in Figure 4A; the locations of the sites, distributed throughout the molecule, are shown in Figure 4B as green spheres. Osmolyte shifts toward the more immobile population (arrows in Figure 4A) are seen for R1 at sites 31, 62, 63, 87, 91, and 106. In the cases of 87R1, 91R1, and 106R1, the population of the immobile component is small in the absence of sucrose, but osmolyte perturbation increases the population sufficiently to be resolved. Although the effects are relatively small, they are of the magnitude expected for osmolyte shifts of conformational equilibria.[19] Sites showing osmolyte shifts are limited to the central region of the B helix, the N terminal region of the E helix, the center of the F helix, and the N terminal region of the G helix (Figure 4B). Models for the conformational substates giving rise to the two-component spectra will be considered in the Discussion section. As expected, the EPR spectra of sites showing a single dynamic state of R1 show no osmolyte shift (Figure S8, Supporting Information).

Overall, the results show that holomyoglobin is well-ordered with limited conformational flexibility in discrete regions of the molecule.

Conformational Flexibility in N_{Apo}. To map changes in conformation that arise in the $N_{Holo} \rightarrow N_{Apo}$ transition, the EPR spectra of the same 38 spin-labeled mutants studied for N_{Holo} were recorded in the N_{Apo} state in Ficoll 70 at pH 6.1. The entire set of spectra is given in Figure S9, Supporting Information, and a subset representing each helix is shown in Figure 5A; the spectra are compared with the same sites in N_{Holo} to illustrate the nature of the changes. Remarkably, 24 of the 38 sites in N_{Apo} show two-component spectra compared to only 10 for N_{Holo}. In each case, the second component corresponds to an immobilized state of the nitroxide, reflecting tertiary interaction with the environment; examples in Figure

dx.doi.org/10.1021/bi3005686 | Biochemistry 2012, 51, 6568−6583

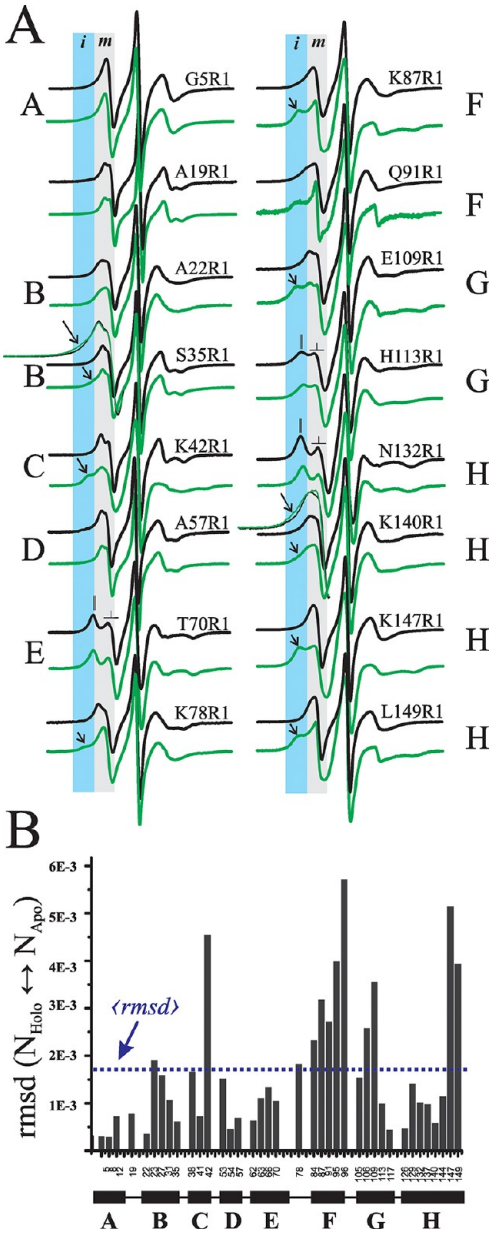

Figure 5. Conformational changes in the $N_{Holo} \rightarrow N_{Apo}$ transition. (A) The EPR spectra of spin-labeled N_{Holo} and N_{Apo} in Ficoll are shown in black and green, respectively. The light blue and gray areas identify regions where relatively immobile and mobile states of the nitroxide, respectively, contribute to the intensity. The symbols ⊥ and ∥ in the spectra of residues 70R1 and 132R1 identify the well-resolved hyperfine components arising due to the anisotropic motion of the nitroxide. The low field region of the spectra of residues 35R1 and 140R1 are amplified and overlaid to show the differences. (B) rmsd of the EPR spectra for each residue between the N_{Holo} and N_{Apo} state. The horizontal bars indicate the location of each site in the high-resolution structure of holomyoglobin (helices A–H). The dashed line shows the overall average rmsd value.

5A include residues at the C-terminus of helix B (35R1), in helix C (42R1), EF turn (78R1), and in helices F (87R1, 91R1), G (109R1), and H (140R1, 147R1, 149R1); other sites showing similar changes in these same helices are highlighted in Figure S9 (Supporting Information). Interestingly, the sharp components in the spectra of R1 in helix F (87R1 and 91R1,) and the C-terminus of helix H (149R1) reflect a high mobility of the backbone ($\tau \sim 1$ ns, $S \leq 0.1$),[19] which may arise from local unfolding or from a helical segment with a high amplitude of spatial reorientation on the ns time scale (see Discussion).

A simple measure to illustrate the site-specific differences between the N_{Holo} and the N_{Apo} is the root-mean-square difference (rmsd) of the normalized EPR spectra. Figure 5B shows rmsd per residue; the average value for all sites is shown by the horizontal dotted line. Above average values of rmsd are observed in four regions of the molecule, namely, residue 23 in helix B, residue 42R1 in helix C, residues 78–109, which correspond to the EF turn, the F-helix, the FG turn, and the first half of G-helix, and residues 147–149 corresponding to the C-terminal region of the H-helix.

To identify which of the multicomponent spectra observed in the N_{Apo} state arise from conformational exchange, the spectra were compared in Ficoll and sucrose solutions. The spectra of all multicomponent sites showing sensitivity to osmolyte perturbation are shown in Figure 6A; the complete data set is provided in Figure S10 (Supporting Information). Fourteen of the 24 multicomponent spectra showed an osmolyte shift toward a more immobile state, identifying those sites as residing in regions of conformational exchange. Interestingly, most of these sites are in the same sequences that exhibit spectral changes between the holo and apo states. This is shown graphically in Figure 6B, where the spheres are color-coded according to the magnitude of the rmsd in the transition from N_{Holo} to N_{Apo}, and the backbone is colored according to regions identified as conformational exchange via osmolyte perturbation. As expected, sites with single-component EPR spectra showed no osmolyte shift (Figure S11, Supporting Information).

Conformational Flexibility in the I_{MG} State. Earlier studies have shown that apomyoglobin at pH 4 in the absence of salt populates a compact equilibrium molten globule state (I_{MG})[29,55] that strongly resembles the obligatory kinetic intermediate formed within 6 ms of the folding pathway of myoglobin.[56,57] To map the changes in conformational flexibility in the transition from N_{Apo} to I_{MG}, the pH of the protein solutions for 37 of the spin-labeled mutants was lowered to 4.1, and the EPR spectra were recorded at 298 K.

Remarkably, the EPR spectra of R1 at every site studied in the I_{MG} state had multiple components, some of which reflected a single component in the N_{Holo} and N_{Apo} states. A subset of the spectra is shown in Figure 7A (blue traces) along with a comparison of the corresponding spectra in the N_{Apo} form (green traces); the complete set of spectra is given in Figure S12 (Supporting Information). In addition to the appearance of immobilized states at many sites, sharp components (arrows) reflecting a high degree of mobility on the nanosecond time scale appear or are increased in population in the spectra for sites within the C, D, E, and F helices (e.g., 41R1, 57R1, 66R1, 70R1, and 84R1). For example, the sharp component in 66R1 can be fit with $\tau \approx 0.7$ ns, $S = 0$ (Table S2, Supporting Information). These parameters are similar to those for disordered sequences tethered to a folded structure,[59,60] suggesting that these helices may sample unfolded conformations. However, the more mobile states for R1 in other helices (i.e., A, B, G, and H) reflect a restricted motion of the backbone. As an example, the component in the spectrum of residue 113R1 corresponding to a mobile state can be reasonably well fit with the MOMD model using $\tau = 2.3$ ns, $S = 0.26$ (Figure S6 and Table S2, Supporting Information),

dx.doi.org/10.1021/bi3005686 | Biochemistry 2012, 51, 6568–6583

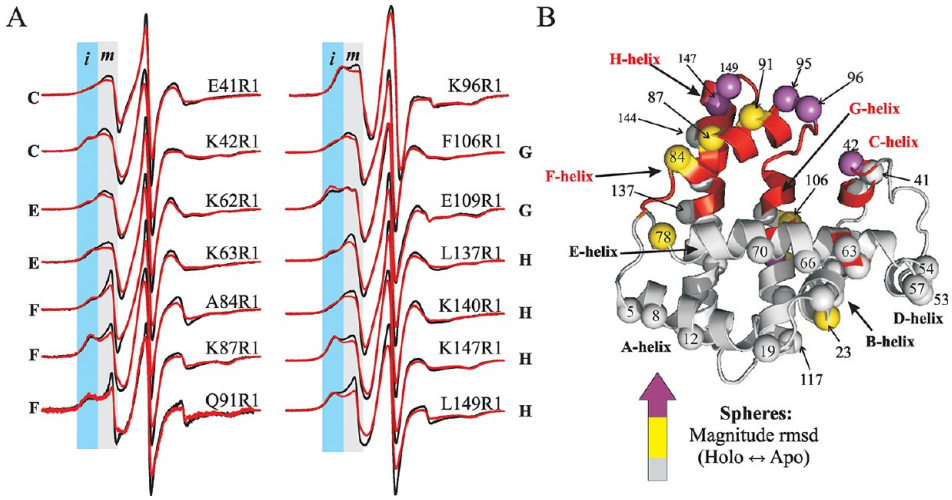

Figure 6. Conformational exchange in N_{Apo}. (A) EPR spectra of R1 at sites exhibiting osmotic shifts. The spectra recorded in Ficoll 70 and in sucrose are shown in black and red, respectively. The light blue and gray areas identify regions where relatively immobile and mobile states of the nitroxide, respectively, contribute to the intensity. (B) Ribbon diagram of myoglobin showing regions identified to be in conformational exchange as a red ribbon and relative rmsd values from Figure 5B as color coded spheres at Cα: gray, rmsd < ⟨rmsd⟩; yellow, ⟨rmsd⟩ ≤ rmsd ≤ ⟨rmsd⟩ + σ; magenta, rmsd > ⟨rmsd⟩ + σ, where σ is the standard deviation from the mean.

which is similar to the values observed for R1 at relatively mobile, noninteracting helix surface sites.

Although soluble aggregates were removed in the purification of the spin-labeled mutants, one might argue that the existence of relatively immobile states in the spectra of R1 at every site in the I_{MG} state is due to the reappearance of aggregates at pH 4. To evaluate this possibility, a set of spin-labeled mutants of myoglobin in the N_{Apo} state (100% monomer) were immobilized on a Sepharose solid support (see Experimental Procedures), and the pH of the solution was lowered from 6.1 to 4.1. Except for the single case of residue A19R1, the EPR spectra of the immobilized proteins in I_{MG} are similar to those in solution (see Figure S13A,B, Supporting Information). Because aggregation cannot occur for the immobilized proteins, it is concluded that the immobile component observed is characteristic of the I_{MG} fold and not due to protein aggregation. Additional evidence for this conclusion is provided by the complete reversibility of the pH induced transitions as detected by EPR (Figure S13C, Supporting Information).

Figure 7B shows the rmsd of the spectra for the N_{Apo} to I_{MG} transition. There are significant changes at most sites; in fact, the average rmsd for the N_{Apo} to I_{MG} transition (red dashed line Figure 7B) is twice that observed for N_{Holo} to N_{Apo} (see black dashed line in Figure 7B). Above average changes in the EPR spectra were observed at sites in helices A, F, the C-terminus of G, and helix H.

The effect of osmolyte perturbation is shown in Figure 8A for representative multicomponent spectra in I_{MG}; the complete data set is provided in Figure S14 (Supporting Information). With few exceptions, there is an osmolyte shift toward the relatively immobilized state, suggesting that I_{MG} at 298 K is conformationally heterogeneous, with helices C, D, E, and F sampling highly dynamic unfolded conformations. These conclusions are summarized graphically in Figure 8B where the spheres representing R1 sites are color-coded according to the magnitude of the rmsd in the transition from N_{Apo} to I_{MG}, and the backbone is coded by color and shape to identify regions involved in conformational exchange and regions sampling unfolded states, respectively.

Structural Changes in the N_{Holo} → N_{Apo} → I_{MG} Transitions Monitored via DEER Spectroscopy. The previous sections were focused on identifying molecular flexibility in myoglobin as probed by CW EPR line shape analysis of singly R1-labeled protein. Complementary structural information can be obtained with distance measurements between pairs of R1 residues using Double Electron−Electron Resonance (DEER) spectroscopy[61,62] that measures the probability distribution of distances between unpaired electrons in the 17−80 Å range for frozen samples at cryogenic temperatures (80 K).[63] The most probable distance and width of the distribution provide direct information on the structure and structural heterogeneity, respectively. The structural heterogeneity is presumably related to the amplitude of molecular motion at physiological temperatures, which has contributions from both R1 motion and the intrinsic protein flexibility.

The DEER experiment measures the magnetic interaction between two unpaired electrons by monitoring the amplitude (A) of an electron spin echo of an observed spin as a function of the time (t) at which a microwave pulse inverts the magnetization of an interacting partner. This primary data is corrected by subtraction of an exponentially decaying background due to random intermolecular dipolar interactions to give the dipolar evolution function (DEF), which in turn is fit to obtain the probability distribution of interspin distances.[62]

Four pairs of R1 mutants were engineered, and the interspin distance distribution was monitored for each in N_{Holo}, N_{Apo}, and I_{MG} using DEER spectroscopy. Figure 9A shows the location of the R1 pairs in myoglobin selected to monitor the distances between helices A and H (12R1/132R1), B and E (31R1/70R1), B and F (31R1/87R1), and D and H (57R1/132R1). Panels B and C in Figure 9 show the DEFs and derived distance distributions, respectively.

The most probable distances for the four pairs in the N_{Holo} state are in close agreement (±1.5 Å) with the predicted interspin distances from modeling the R1 side chain in the high resolution structure (Table S3, Supporting Information). The distribution widths are relatively narrow in N_{Holo} for 12R1/132R1 and 31R1/70R1, consistent with single conformations of

dx.doi.org/10.1021/bi3005686 | Biochemistry 2012, 51, 6568−6583

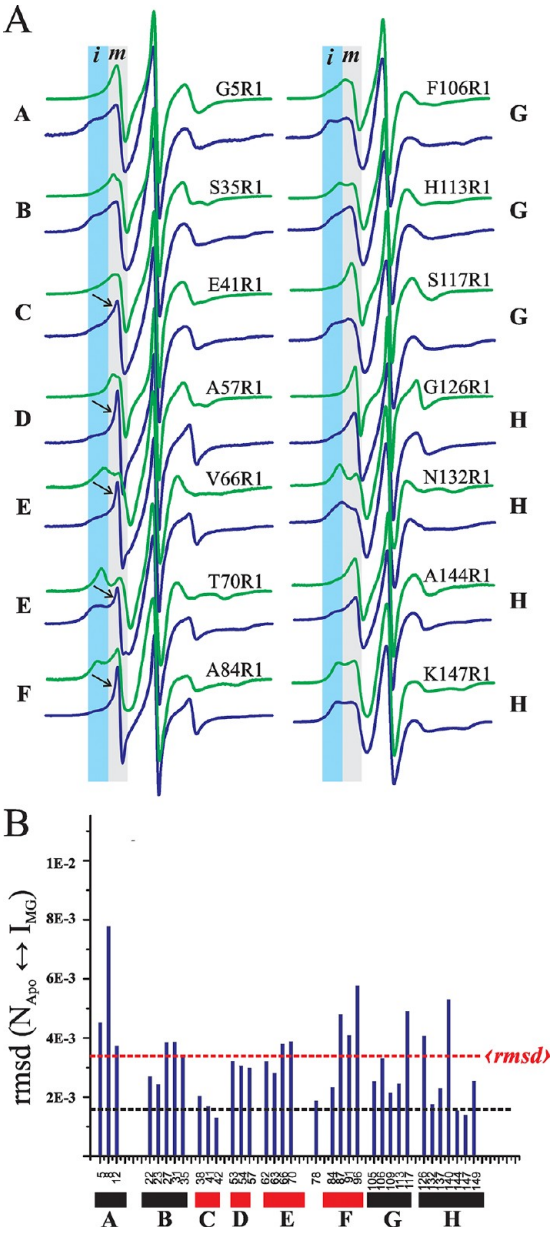

Figure 7. Conformational changes in the $N_{Apo} \rightarrow I_{MG}$ transition. (A) Representative EPR spectra of N_{Apo} (green traces) and I_{MG} (blue traces) recorded in Ficoll 70. The light blue and gray areas identify regions where relatively immobile and mobile states of the nitroxide, respectively, contribute to the intensity. The helices in which the R1 side chains are located are indicated. The arrows identify sharp spectral components reflecting high mobility of the backbone (see text). The EPR spectra of residues 41R1 and 66R1 in N_{Apo} and I_{MG} states in Ficoll have been previously reported[58] and are reproduced here. Reprinted from ref 58. Copyright 2011 American Chemical Society. (B) The rmsd of the EPR spectra between the N_{Apo} and I_{MG} state. The horizontal dashed line shows the overall average rmsd value. The average rmsd between the N_{Holo} and N_{Apo} states is shown for comparison (see black dashed line). The horizontal bars indicated the location of each site in the high-resolution structure of holo myolglobin (helices A–H). The horizontal red bars identify the regions in which the EPR spectra show a highly mobile state of the nitroxide side chain.

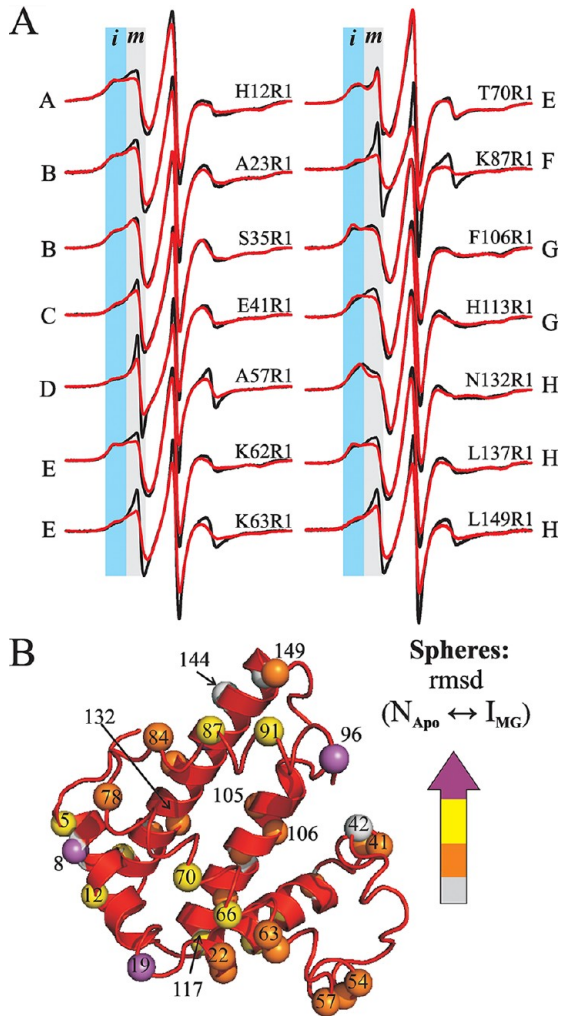

Figure 8. Conformational exchange in I_{MG}. (A) Representative spectra recorded in Ficoll 70 (black) and sucrose (red) are superimposed. The light blue and gray areas identify regions where relatively immobile and mobile states of the nitroxide, respectively, contribute to the intensity. (B) Ribbon diagram of myoglobin showing sequences believed to be in conformational exchange in red (the entire molecule). The thin tube representation of the backbone identifies sequences that sample unfolded conformations (see text). The spheres at the Cα are color coded according to the magnitude of rmsd between the N_{Apo} and I_{MG} states (data from Figure 7B) gray, below ⟨rmsd⟩ holo to apo (below dashed black line); orange, ⟨rmsd⟩ ≤ rmsd apo to MG; yellow, ⟨rmsd⟩ ≤ rmsd ≤ ⟨rmsd⟩ + σ; magenta, rmsd > ⟨rmsd⟩ + σ, where σ is the standard deviation from the mean.

the A, B, E, and H helices, at least in the vicinity of the labels. However, the distance distribution for 31R1/87R1 is broader and asymmetric by comparison, implying a greater structural heterogeneity of helix F in which 87R1 resides. This conclusion is consistent with the conformational exchange involving helix F identified by the osmolyte perturbation. Interestingly, the distance distribution for the 57R1/132R1 pair in the N_{Holo} state is bimodal, with a second population shifted by about +5 Å from the most probable distance. This may reflect a second position for the short and flexible D helix but could also arise from a second rotamer of R1 (see Discussion).

The distribution of distances sampled by 12R1/32R1, 31R1/70R1, and 57R1/132R1 in the N_{Apo} state are very similar to those in the N_{Holo} form (Figure 9C), indicating little change in the overall tertiary fold sampled by these pairs. Although there is no change in the most probable distance for the 31R1/70R1 pair, the width of the distance distribution observed in the N_{Apo} state is greater by ≈5 Å (Table S3, Supporting Information),

dx.doi.org/10.1021/bi3005686 | Biochemistry 2012, 51, 6568–6583

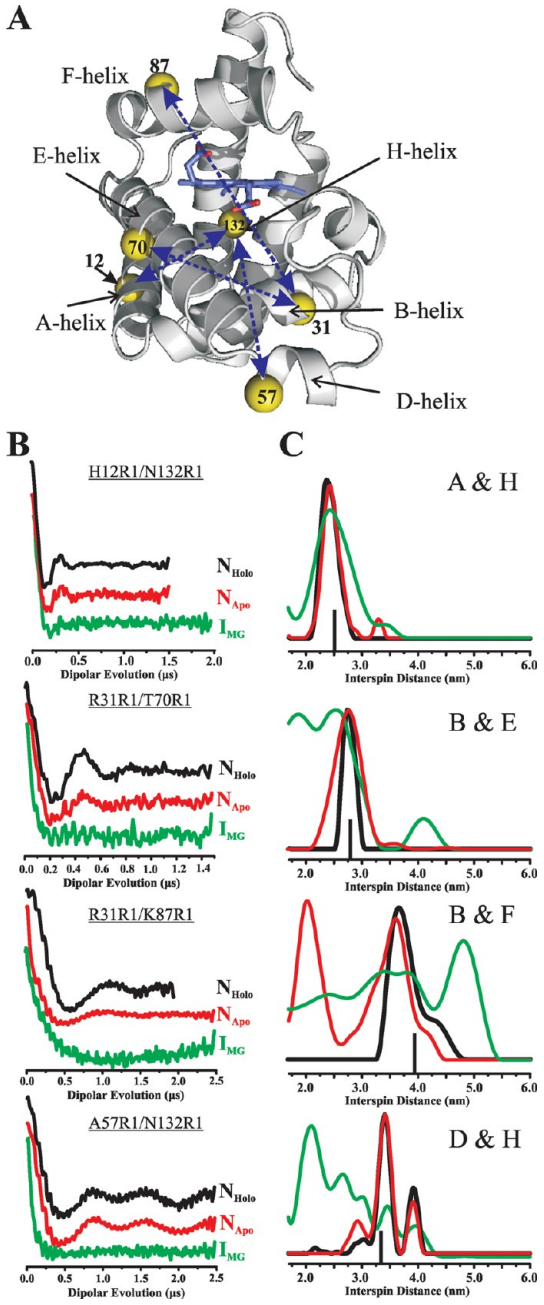

Figure 9. Monitoring structural changes in the $N_{Holo} \rightarrow N_{Apo} \rightarrow I_{MG}$ transitions with DEER spectroscopy. (A) Ribbon diagram showing the location of R1 sites from which pairs were selected to monitor the indicated distances. (B) Dipolar evolution functions for the indicated mutants in the N_{Holo}, N_{Apo}, and I_{MG} states, and (C) the corresponding interspin distance distributions. The vertical black bars indicate the predicted interspin distance from modeling the R1 side chains in the high resolution structure of N_{Holo} (see Supporting Information).

likely reflecting higher structural flexibility in the N_{Apo} state. The interspin distance distribution for the 31R1/87R1 pair showed a dramatic change in the $N_{Holo} \rightarrow N_{Apo}$ transition wherein the distance distribution between the B and F helices monitored by this pair becomes bimodal with a long distance similar to that observed in the holo form (36 Å) and a new interspin distance with maximum at 20 Å. Because there is no change in the most probable distance and only a slight change in distribution width for the 31R1/70R1 pair, the origin of the bimodal distribution for the 31R1/87R1 pair must reside in movement of 87R1 in the F helix. A model to account for the striking change in distance distribution will be considered in the Discussion.

Upon formation of the I_{MG}, all R1/R1 distance distributions are dramatically broader than those in the N_{Holo} and N_{Apo} states, reflecting a structural heterogeneity consistent with the conformational exchange at physiological temperatures revealed by the osmolyte perturbation response presented in Figure 8. It is emphasized that due to the relatively low signal-to-noise ratio and featureless modulation for some of the data in the molten globule state (e.g., R31R1/T70R1) there is uncertainty in the detailed shape of the distribution profiles.

DISCUSSION

The overall aim of the present study was to explore the potential of SDSL to identify protein flexibility with characteristic times ranging from ns to ms and longer. Data presented in this study extend earlier work[17] and suggest that R1 motion in ordered helices can be analyzed to infer relative ns-scale motions of helical segments to which the nitroxide is attached.

Conformational exchange between substates is typically in the μs−ms range, at least an order of magnitude outside the intrinsic CW EPR time window. One goal of the present study was to elucidate how conformational flexibility is revealed in the EPR spectra and to verify the osmolyte perturbation strategy in SDSL for mapping of conformational flexibility using myoglobin as a test case. The results establish an interesting principle, namely, that conformational flexibility, involving exchange between substates with characteristic lifetimes in the μs−ms range, may be revealed by components in the EPR spectrum corresponding to immobilized states of R1. The fact that flexibility is revealed by immobilization of R1 is due to the fast time scale of the EPR experiment relative to the protein motions. The lifetime of the individual conformational substates is long on the EPR time scale, so the ≈1 ns internal motions of R1 allow the side chain to fully explore the local environment in each substate. In some of the substates, the local conformation can be such that R1 experiences immobilizing contacts with other parts of the structure as depicted in Figure 10A where the substates are related by a simple repositioning of helical segments.

However, the presence of a conformational substate that involves a locally unfolded sequence or one with a highly mobile secondary structural element will give rise to a sharp spectral component in the CW EPR spectrum corresponding to a highly mobile state of R1 (see Figure 10B). Details of the results leading to the above conclusions are discussed below with respect to each of the 3 equilibrium states of myoglobin together with comparisons of SDSL and relevant NMR data.

Monitoring Nanosecond Backbone Flexibility in Well-Ordered Helices of Holo Myoglobin. The utility of SDSL-EPR to detect ns backbone fluctuations has been demonstrated in earlier studies on the relatively unstable helices of GCN4,[17] which have been found in NMR studies to sample nonhelical conformations with large amplitude internal backbone motions on the ps−ns time scale.[64] Such large amplitude motions on this time scale give rise to sharp, distinctive EPR spectral line shapes that are diagnostic for this condition.[17] In addition to GCN4, the SDSL-EPR method has been employed to identify disordered sequences in other proteins, including membrane proteins.[16,65,66]

In contrast to these highly flexible sequences, the EPR spectra of R1 on the solvent exposed surfaces of well-ordered

dx.doi.org/10.1021/bi3005686 | Biochemistry 2012, 51, 6568−6583

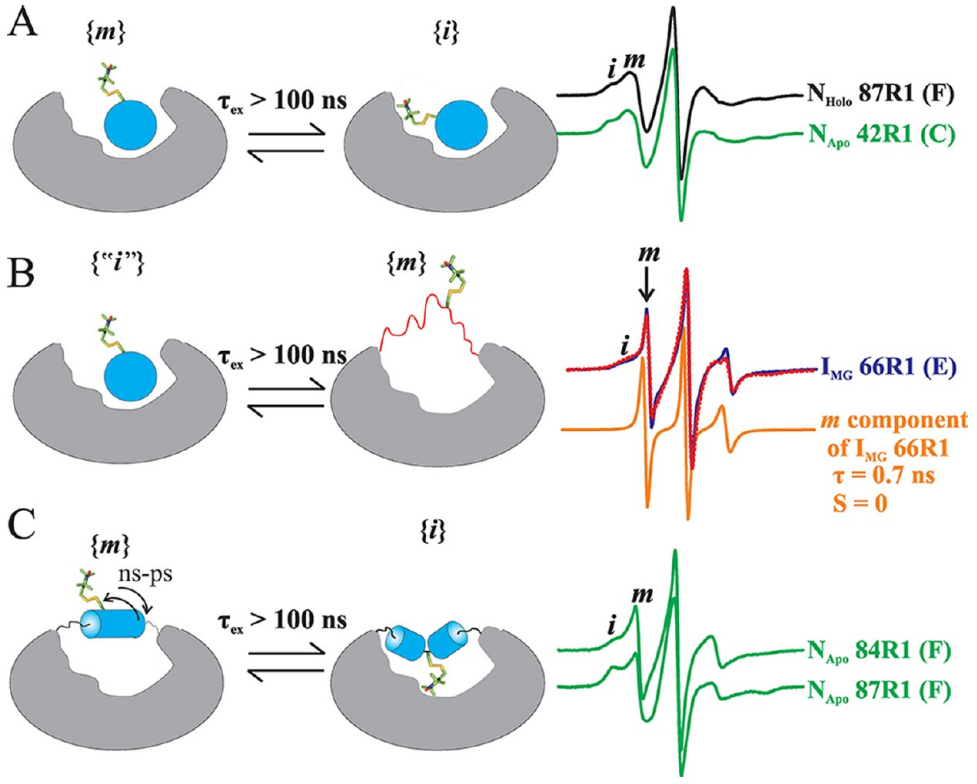

Figure 10. Schematic representation of substates that could give rise to the multicomponent EPR spectra observed in the N_{Holo}, N_{Apo}, and I_{MG} states of myoglobin. For each scenario, candidates from myoglobin experimental data are shown in the right panel (see text). (A) Helical motion on the μs−ms time scale brings the nitroxide into tertiary contact with the protein environment in one substate, giving rise to a relatively immobile state of R1. (B) Exchange between a highly mobile state of R1 arising from an unfolded polypeptide chain with high backbone flexibility and a more ordered state(s) giving rise to a second relatively immobile component (see text below). Spectral simulation (red dashed lines) and the deconvoluted mobile component obtained from the fit (orange) of the spectrum of residue 66R1 in the I_{MG} state are shown. (C) Exchange between a highly dynamic helical segment and a second substate where the F-helix sequence collapses into the heme pocket to give rise to the relatively immobilized nitroxide. It is noted that there is an uncertainty as to the nature of the secondary structure of the F-helix sequence in the collapsed substate.

stable helices, as judged, for example, by high protection factors in hydrogen/deuterium exchange data, exhibit broader lines reflecting anisotropic constrained motions. Nevertheless, there are variations in the motion from site to site as shown in Figure 2. A question arises as to the origin of these variations. On the one hand, the site-to-site variations in the spectra of R1 could reflect subtle differences in the local backbone motion. On the other hand, in principle, site-specific differences in R1 rotamers, rotamer exchange, and/or local interactions in the protein could also account for variations in EPR spectra of the kind shown in Figure 2.[18,67] Mutagenesis experiments have ruled out interactions with neighboring side chains in the same helix as the source of variation for R1 at solvent exposed sites in stable helices of T4L.[14,46]

Numerous studies have shown a link between the amplitude of backbone motions and local packing in proteins.[68−72] The correlation of M_s and the rate and order of R1 motion with f_{buried} as a measure of the number of local contacts (Figure 3A and B) is consistent with this result and supports a model in which the variation of motion of R1 from site to site in helical sequences has an important contribution from ns backbone flexibility.

In further support of this model are correlations of the EPR, crystallographic, and NMR data. For example, the high $\langle M_s \rangle$ for the short helix D in N_{Holo} (Figure 3C) are consistent with relatively high B-factors for Cα in the high-resolution structure[73] and the low $\{^1H\}$-^{15}N NOE values which reflect large amplitude ps−ns time scale motions of the backbone.[29] In addition, crystallographic studies of N_{Holo} at variable temperature revealed a considerable volumetric expansion of the sequence corresponding to helices C and D with increasing temperature, which implies greater plasticity for this region.[74] In this regard, the average $\langle M_s \rangle$ value for helix C is the second highest among the 8 helices. Of particular interest is the clear gradient of motion observed for R1 along helix H, increasing toward the C-terminus, which is inversely correlated to f_{buried} (Figure 3D). The high-resolution structure of myoglobin shows a gradient of B-factor values along the same sequence (Figure S7, Supporting Information) increasing toward the C-terminus,[1,73] while different high-resolution structures of myoglobin show plasticity beyond residue 146 (Figure S7, Supporting Information). Finally, $\{^1N\}$-^{15}H heteronuclear NOE measurements appear to show a gradient, albeit within the noise level of the measurement, along the same sequence.[29]

The details of the dynamic mode of backbone motion that is sensed by R1 remains uncertain, but the EPR spectra of R1 are primarily sensitive to motions of a helical segment that result in reorientation of the 2p orbital of the nitroxide (e.g., rocking motions), which lies approximately perpendicular to the helical axis in the favored R1 rotamers.[16] The NMR S^2_{NH} order parameter determined by ^{15}N relaxation measurements is not expected to be sensitive to rocking motions of a helix because the N−H bond vector is collinear with the helical axis. Rather, S^2_{NH} is apparently modulated by a "crankshaft" motion that

dx.doi.org/10.1021/bi3005686 | Biochemistry 2012, 51, 6568−6583

results in fluctuations of the N−H bond vector[75] but does not reorient local side chains, including R1. Thus, a strong correspondence of EPR line shape effects and the NMR S^2_{NH} parameter is not necessarily expected, but the distinct motions may be correlated as a result of a common structural origin.

For simplicity, the analysis of backbone motion in this work has been restricted to sites reflecting simple one-component spectra in N_{Holo}; however, a similar analysis could be carried out for sites reflecting two-component spectra by using spectral simulations. In such cases, the more mobile component is expected to arise from states of the side chain not in tertiary contact with neighboring residues and hence should reflect contributions from backbone motions. Taken together with earlier work,[16,17] the data presented here shows the capability of SDSL-EPR as a general method for mapping backbone dynamics of disordered and well-ordered protein sequences in the ps−ns range.

Mapping Conformational Exchange in Proteins: Folded and Partially Folded States of Myoglobin. *N_{Holo} State.* For the majority of sites studied in N_{Holo}, the spectra of R1 have a single component consistent with relatively low amplitude backbone motions on the ps−ns time scale (Figure 2). The paucity of two-component spectra by itself suggests a rigid tertiary fold, which is consistent with the narrow distance distributions between the R1 pairs investigated (Figure 9). Notable exceptions are the two-component spectra of residues 87R1 and 91R1 in the F helix, 62R1 and 63R1 at the N-terminus of helix E, and 106R1 in the G-helix, each of which was attributed to conformational flexibility by the osmotic perturbation criterion. The spectra of residues 84R1 and 96R1, at the ends of the F-helix (96R1 has a single component spectrum, Figure S8, Supporting Information), are insensitive to osmotic perturbation, suggesting that the conformational exchange detected by residues 87R1 and 91R1 is localized to the central region of the F helix. Interestingly, the sequence near residues 87 and 91 contains a proline at position 88 which may be responsible for the conformational flexibility observed. In addition, residues 87 and 91 are close to His 93, which is directly bound to the heme group. Hence, it is possible that the localized conformational exchange identified on the F-helix may be functionally significant given that this region has shown plasticity upon binding of different ligands to the heme iron.[1,76,77]

Although multiple conformations in any of the aforementioned sequences were not specifically discussed in NMR reports for the N_{Holo} state,[29] the EPR data is compatible with that from NMR. The $^{13}C\alpha$ resonances for residues 86−87 of the F-helix were not assigned in the NMR studies,[38] and the average $^{13}C\alpha$ chemical shift value for the residues in the center of the helix (88−90) are low relative to those in other helices. In addition, H/D exchange experiments revealed low protection factors for several amides within the F-helix. Thus, it is plausible that helix F sample states with distorted geometry with lifetimes shorter than milliseconds, a situation that would give population-weighted average chemical shifts, but resolved components on the EPR time scale. We have in mind a situation such as that in Figure 10A where one of the different positions that the helix samples leads to tertiary contacts of R1; helical distortions, aided by proline 88, may be required to reach the position in tertiary contact.

Residues 62−63 in helix E have $^{13}C\alpha$ chemical shifts values and protection factors characteristic of residues in well-ordered helices. However, submillisecond exchange of the helical segment containing 62 and 63 between states differing only in position of the segment may not be detected in the averaged chemical shift data, particularly since $^{13}C\alpha$ shifts are predominantly determined by backbone structure. However, the R1 side chain is extremely sensitive in the detection of such substates due to the short-range nature of intermolecular attractive interactions[78] ($1/r^6$) that lead to the appearance of immobilized components. Thus, even subtle structural changes can bring the nitroxide into a productive interaction.

It should be noted that the relative population of the second conformation giving rise to the immobilized state for most sites exhibiting sensitivity to osmolyte perturbation is relatively low (≤10%) as determined by spectral simulation (Table S2 and Figure S6, Supporting Information). Thus, it is likely that the NMR methods used in earlier studies were not sufficiently sensitive to detect exchange between a highly populated ground state and a transiently populated state.

The origin of the two discrete distances of narrow width observed between residues 57R1 and 132R1 in helices D and H (Figure 10), respectively, remains to be determined. However, the origin of the bimodal distribution likely lies in residue 57R1 in helix D since the distance distribution between another pair involving 132R1 is monomodal as depicted in Figure 9. Whether the bimodal distance distribution for the 57R1/132R1 pair represents two positions of helix D or two rotamers of 57R1 will be determined in future experiments using a conformationally constrained nitroxide side chain and a double resonance experiment that monitors spatial reorientations of a helix under physiological conditions.[15]

N_{Apo} State. The most striking feature of the difference between N_{Holo} and N_{Apo} is the appearance of two-component spectra for R1 in N_{Apo} at multiple sites; in each case, an osmotic shift confirms conformational exchange. Of particular interest is the F helix in N_{Apo}, where NMR resonances for the entire sequence 81−102 are undetected, presumably due to conformational exchange on the ms time scale.[29] However, on the EPR time scale, the states contributing to the apparent exchange are resolved by R1. At each site in the F helix investigated here and elsewhere,[19] the spectra reflect a dominant immobilized state in addition to a second population (∼15−25%) exhibiting narrow resonance lines diagnostic of a highly flexible backbone. For example, fits to the 87R1 spectrum to the MOMD model give τ = 1.3 ns and S = 0.1 for the mobile component.[19]

Insight into the structural origin of the two-component spectra observed for sites in helix F in N_{Apo} was obtained from the interspin distance distribution between the reference 31R1 in helix B and 87R1 in helix F, which reveals a bimodal distance distribution. The relatively broad interspin distance of 40 Å is similar to that observed in the N_{Holo} state while the shorter distance near 20 Å can only be satisfied by a second population whereby the 87R1 side chain is buried in the now empty heme cavity. Thus, the substate giving rise to the short interspin distance and to the more immobilized state of the nitroxide likely represents a state where the heme pocket is filled or partially filled with the F-helix sequence. In accord with the above interpretation, radical footprinting studies[79] and recent relaxation dispersion NMR data[24] both suggest that the heme binding site is partially occupied in the apo state, likely by the flexible F-helix sequence. The 40 Å distance then likely corresponds to the more mobile state of R1 at ambient temperature. The relatively broad distribution is consistent with static disorder of a helical segment but not with a disordered

dx.doi.org/10.1021/bi3005686 | *Biochemistry* 2012, 51, 6568−6583

coil state, which would have a much broader distribution.[80] Collectively, the data suggest the model shown schematically in Figure 10C, where large amplitude fluctuations of a native-like F helix give rise to the mobile state, and the immobile state arises from a second substate where the sequence is partially buried in the heme cavity. Simulations show that helix fluctuations of amplitude ≈15° on the ns time scale could give rise to a line shape similar to that observed for the mobile component, as illustrated in Figure 10C. It is noted that there is not enough evidence from our study to establish whether the collapsed state of the F-helix sequence is helical or distorted/unfolded.

In addition to R1 sites in helix F, R1 at sites located in helices C, E, G, and H have two-component EPR spectra that appear in the transition from N_{Holo} to N_{Apo} and show osmolyte shifts (Figure 6). To a large extent, these are in sequences that overlap with those identified by NMR to be in conformational exchange. For instance, the NMR resonances for $^{13}C\alpha$, ^{1}H, and ^{15}N were not observed in residues 144−148 at the C-terminus of helix H, attributed to conformational exchange on the ms time scale.[28,29] Recent NMR relaxation dispersion measurements of N_{Apo} revealed additional exchange processes for residues in the sequences 103−108 in the F−G loop and the N terminus of helix G, and in 136−152 in the H helix with exchange lifetimes less than about 500 ms.[24] Moreover, similar exchange rates were found for residues in the sequence 38−42 corresponding to helix C. Comparison with Figure 6B shows that there is excellent agreement between the NMR and SDSL-EPR data regarding the assignment of conformational exchange.

The NMR and EPR data suggest that the conformational exchange observed in the C, E, G, and H helices extends to sites beyond those in direct contact with the conformationally disordered helix F. For example, osmolyte shifts are detected in two-component spectra for R1 residues along an extended solvent-exposed surface of helix H directly opposite that in contact with F (137R1 to 147R1); the most distal of these residues is a full turn from the nearest contact with helix F. Similar arguments can be made for helix G, where R1 residues along the solvent exposed surface that extend 2 turns away from F sense local packing changes (102−109). These results argue for fluctuations in the N_{Apo} structure delocalized from sites in direct contact with helix F. Further evidence for such fluctuations may be found in the reduced values of the $^{13}C\alpha$ shifts for 38−42, 102−109, and 137−144 in N_{Apo} relative to N_{Holo},[29] suggesting the presence of states with distorted backbone geometry in exchange, perhaps on a μs time scale, with the native helical state.

The fluctuations of the protein fold sensed by R1 in helices other than F may involve states such as those shown in Figure 10A. As applied to the N_{Apo} state, the more mobile component arises from R1 at a solvent-exposed helical site similar to its counterpoint in N_{Holo}, while the relatively immobilized component likely corresponds to a displacement or distortion of the helix that brings R1 into contact with other elements of the fold.

I_{MG} State. The transition from N_{Apo} to I_{MG} is remarkable in that the spectra for R1 at every site analyzed reflect two resolved components, many of which were single-component in the N_{Apo} state. Osmolyte shifts suggest that for most sites the multicomponent spectra arise from conformational exchange between at least two states. The mobility of the nitroxide in each of the resolved spectral components provides insights into the backbone flexibility and structure of each of the conformational states in equilibrium. For example, in cases where the more mobile component of the spectrum reflects constrained motion of the backbone (i.e., $\tau > 1$ ns and $S > 0$), it is likely that the substates involved have a folded structure. This appears to be the case for residues within the sequences corresponding to helices A, B, G, and H in the native state. As an example, the more mobile component of residue 113R1, located in helix G, can be reasonably fit with $\tau = 2.3$ and $S = 0.26$, which are comparable to those values observed for R1 in folded helical structures[13,14] including those in the N_{Holo} state (Figure S7 and Table S2, Supporting Information).

The EPR data depict a very different situation for residues within the C, D, E, and F regions. On each of these helices, most of the spectra of R1 have a resolved component that reflects a fast, essentially isotropic, motion likely arising from a flexible random coil state. For example, the more mobile component on the spectrum of 66R1 located on helix E, can be reasonably fit with isotropic motion (i.e., $S = 0$) and $\tau = 0.7$ ns (Figure S6 and Table S2, Supporting Information), which is comparable to τ values observed in unfolded protein sequences.[59,60]

Differences in the conformational flexibility of the A−B−G−H and the C−D−E−F sequences in the I_{MG} state can also be inferred from the DEER data. Although the DEER data set is limited, qualitative differences were observed in the distance distribution between pairs involving sites within helices A and H, and those involving sites located in helices D, E, and F (Figure 9). For example, the width of the distance distribution for the 12R1/132R1 pair, located in helix A and H, respectively, is narrower than those of the other three pairs, which include sites 57R1, 70R1, and 87R1, located in helices D, E, and F, respectively. In addition to the narrower distance distribution, the 12R1/132R1 pair has a monomodal distribution, while the distribution on the other three pairs reflect multiple peaks, presumably corresponding to different positions of the backbone.

Thus, the EPR data collectively suggest that the entire I_{MG} structure is conformationally heterogeneous on the EPR time scale with exchange lifetimes longer than about 100 ns. Importantly, the data reveal that helices C−D−E and F explore nonhelical states with dynamically disordered backbones, while the A−B−G−H core helices apparently retain folded structures. These findings are entirely consistent with NMR data on the I_{MG} state.[29,32] In particular, backbone chemical shifts, low temperature coefficients for H^N chemical shifts, and relatively high heteronuclear NOEs all point to a substantial content of helical structure with a low amplitude of fast backbone dynamics in A, the C-terminal end of B, G, and H. NMR relaxation parameters revealed restricted ns mobility of the backbone in the A−B−G−H sequence but with higher amplitudes of motion on a slower (μs) time scale, perhaps reflecting rigid body rotational diffusion of a compact unit, and possibly conformational exchange.[29,32] In regard to the C, D, E, and F sequence, the data from $^{13}C\alpha$ backbone chemical shifts, temperature coefficients for H^N chemical shifts, and reduced heteronuclear NOEs revealed that the C−D−E sequence has lower helical content and higher amplitude of fast backbone dynamics compared to those of the A−B−G−H helices.[29,32]

Although the helices A, B, G, and H maintain much of the secondary structure of N_{Holo} and N_{Apo} in I_{MG},[29,32] they are nevertheless involved in conformational exchange, as suggested by both the NMR and EPR data. One model consistent with the data is a conformational ensemble of these helices in the

dx.doi.org/10.1021/bi3005686 | *Biochemistry* 2012, 51, 6568−6583

I_{MG} state involving substates such as those shown in Figure 10A wherein regular helices fluctuate between positions. The remaining sequences in helices C, D, E, and F may involve a similar ensemble of states but also include a dynamically disordered state, such as that shown in Figure 10B.

SUMMARY AND FUTURE PROSPECTS

By way of comparison with extensive data from NMR and other methodologies on myoglobin, the results of this study demonstrate the utility of CW line shape analysis to map local ns backbone motions and, in combination with osmolyte perturbation, to identify regions in μs−ms conformational exchange in proteins. As a result of the intrinsic EPR time scale, such conformational exchange does not result in spectral averaging, and the individual components corresponding to the substates in equilibrium can be determined by spectral simulation. The individual components in turn provide specific information on the local tertiary fold and backbone dynamics of the substates.[14,17,22,23,43,44,46] Thus, SDSL-EPR is a facile approach for studying the structure and dynamics of highly heterogeneous sequences such as MG states and intrinsically disordered proteins. Although the osmotic perturbation method employed here to map conformational exchange has the advantage of simplicity, the method does not provide the exchange rate between substates. For this purpose, pulsed saturation recovery (SR) EPR[20] and pulsed electron−electron double resonance (ELDOR)[15] can be employed to measure exchange with characteristic times in the range of 1−70 μs. Given the high sensitivity of EPR spectroscopy, exchange on a ms and longer time scale can in principle be determined in real time by perturbation spectroscopy. High pressure EPR[21] and pressure-jump EPR are currently being explored for this purpose.

ASSOCIATED CONTENT

Supporting Information

Entire EPR data set in each of the states, gel filtration profiles for the WT and a set of cysteine mutants, CD spectroscopy data, UV−vis data of holomyoglobin R1 mutants, MOMD fits, and the most probable interspin distance and distance distribution. This material is available free of charge via the Internet at http://pubs.acs.org.

AUTHOR INFORMATION

Corresponding Author

*Tel: (310) 206-8830. E-mail: hubbellw@jsei.ucla.edu.

Funding

This study was supported by NIH Grant number: 5R01 EY005216 and the Jules Stein Professor Endowment.

Notes

The authors declare no competing financial interest.

ACKNOWLEDGMENTS

We thank Dr. Christian Altenbach and Michael Lerch for careful reading of the manuscript. We also thank Dr. Peter E. Wright for helpful comments and Dr. Joseph Horwitz for technical assistance in the use of the CD spectrometer.

ABBREVIATIONS USED

SDSL, site-directed spin labeling; EPR, electron paramagnetic resonance; DEER, double electron−electron resonance; NMR, nuclear magnetic resonance; CW, continuous wave; M_s, scaled mobility; rmsd, root mean squared difference; MOMD, microscopic order−macroscopic disorder

REFERENCES

(1) Hartmann, H., Parak, F., Steigemann, W., Petsko, G. A., Ponzi, D. R., and Frauenfelder, H. (1982) Conformational substates in a protein: Structure and dynamics of metmyoglobin at 80K. *Proc. Natl. Acad. Sci. U.S.A. 79*, 4967−4971.

(2) Frauenfelder, H., Sligar, S. G., and Wolynes., P. G. (1991) The energy landscapes and motions on proteins. *Science 254*, 1598−1603.

(3) Henzler-Wildman, K., and Kern, D. (2007) Dynamic personalities of proteins. *Nature 450*, 964−972.

(4) Woodside, D. G. (2002) Dancing with multiple partners. *Sci. STKE 2002*, pe14.

(5) Lange, O. F., Lakomek, N., Farès, C., Schröder, G. F., Walter, K. F. A., Becker, S., Meiler, J., Grubümller, H., Griesinger, C., and de Groot, B. L. (2008) Recognition dynamics up to microseconds revealed from an RDC-derived ubiquitin ensemble in solution. *Science 320*, 1471−1475.

(6) Ma, B., Shatsky, M., Wolfson, H. J., and Nussinov, R. (2002) Multiple diverse ligand binding at a single protein site: a matter of pre-existing populations. *Protein Sci. 11*, 184−197.

(7) Kumar, S., Ma, B., Tsai, C. J., Sinha, N., and Nussinov, R. (2000) Folding and binding cascades: Dynamic landscapes and population shifts. *Protein Sci. 9*, 10−19.

(8) Boehr, D. D., Nussinov, R., and Wright, P. E. (2009) The role of dynamic conformational ensembles in biomolecular recognition. *Nat. Chem. Biol. 5*, 789−796.

(9) Wright, P. E., and Dyson, H.J.. (2009) Linking folding and binding. *Curr. Opin. Struct. Biol. 19*, 31−38.

(10) Boehr, D. D., Dyson, J. H., and Wright, P. E. (2006) An NMR perspective on enzyme dynamics. *Chem. Rev. 106*, 3055−3079.

(11) Mittermaier, A, and Kay., L. E. (2006) New tools provide new insights in NMR studies of protein dynamics. *Science 312*, 224−228.

(12) Mchaourab, H. S., Kálai, T., Hideg, K., and Hubbell, W. L. (1999) Motion of spin-labeled side chains in T4 lysozyme. Effect of side chain structure. *Biochemistry 38*, 2947−2955.

(13) Columbus, L., Kálai, T., Jeko, J., Hideg, K., and Hubbell, W. L. (2001) Molecular motion of spin-labeled side chains in alpha-helices:analysis by variation of side chain structure. *Biochemistry 40*, 3828−3846.

(14) Fleissner, M. R., Cascio, D., and Hubbell, W. L. (2009) Structural origins of weakly ordered motion in spin-labeled proteins. *Protein Sci. 18*, 893−908.

(15) Fleissner, M. R., Bridges, M. D., Brooks, E. K., Cascio, D., Kálai, T., Hideg, K., and Hubbell, W. L. (2011) Structure and dynamics of a conformationally constrained nitroxide side chain and applications in EPR spectroscopy. *Proc. Natl. Acad. Sci. U.S.A. 108*, 16241−16246.

(16) Columbus, L, and Hubbell, W. L. (2002) A new spin on protein dynamics. *TiBS 27*, 288−295.

(17) Columbus, L., and Hubbell, W. L. (2004) Mapping backbone dynamics in solution with site-directed spin labeling: GCN4−58 bZip free and bound to DNA. *Biochemistry 43*, 7273−7287.

(18) Sezer, D., Freed, J. H., and Roux, B. (2009) Multifrequency electron spin resonance of a spin-labeled protein calculated from molecular dynamics simulations. *J. Am. Chem. Soc. 131*, 2597−2605.

(19) López, C. J., Fleissner, M. R., Guo, Z., Kusnetzow, A. K., and Hubbell, W. L. (2009) Osmolyte perturbation reveals conformational equilibria in spin-labeled proteins. *Protein Sci. 18*, 1637−1652.

(20) Bridges, M. D., Hideg, K., and Hubbell, W. L. (2010) Resolving conformational and rotameric exchange in spin-labeled proteins using saturation recovery EPR. *Appl. Magn. Reson. 37*, 363−390.

(21) McCoy, J., and Hubbell, W. L. (2011) High-pressure EPR reveals conformational equilibria and volumetric properties in spin-labeled proteins. *Proc. Natl. Acad. Sci. U.S.A. 108*, 1331−1336.

(22) Guo, Z., Cascio, D., Hideg, K., Kálai, T., and Hubbell, W. L. (2007) Structural determinants of nitroxide motion in spin-labeled proteins: Tertiary contact and solvent-inaccessible sites in helix G of T4 lysozyme. *Protein Sci. 16*, 1069−1086.

(23) Guo, Z., Casio, D., Hideg, K., and Hubbell, W. L. (2008) Structural determinants of nitroxide motion in spin-labeled proteins: Solvent-exposed sites in helix B of T4 lysozyme. *Protein Sci. 17*, 228–239.
(24) Meinhold, D., and Wright, P. E. (2011) Measurements of protein unfolding/refolding kinetics and structural characterization of hidden intermediates by NMR relaxation dispersion. *Proc. Natl. Acad. Sci. U.S.A. 108*, 9078–9083.
(25) Brucker, E. A., Olson, J. S., Phillips, G. N., Jr., Dou, Y., and Ikeda-Saito, M. (1996) High resolution crystal structures of the deoxy, oxy, and aquomet forms of cobalt myoglobin. *J. Biol. Chem. 271*, 25419–25422.
(26) Vojtechovsky, J., Chu, K., Berendzen, J., Sweet, R. M., and Schlichting, I. (1999) Crystal structures of myoglobin-ligand complexes at near-atomic resolution. *Biophys. J. 77*, 2153–2174.
(27) Ösapay, K., Theriault, Y., Wright, P. E., and Case, D. E. (1994) Solution structure of carbomonoxy myoglobin determined from nuclear magnetic resonance distance and chemical shifts constraints. *J. Mol. Biol. 244*, 183–197.
(28) Eliezer, D., and Wright, P. (1996) Is apomyoglobin a molten globule? Structural characterization by NMR. *J. Mol. Biol. 263*, 531–538.
(29) Eliezer, D., Yao, Y., Dyson, H. J., and Wright, P. (1998) Structural and dynamic characterization of partially folded states of apomyoglobin and implications for protein folding. *Nature Struct. Biol. 5*, 148–155.
(30) Lecomte, J. T. J., Kao, Y. H., and Cocco, M. J. (1996) The native state of apomyoglobin described by proton NMR spectroscopy: The A-B-G-H interface of wild-type sperm whale apomyoglobin. *Proteins 25*, 267–285.
(31) Cavagnero, S., Theriault, Y., Narula, S. S., Dyson, H. J., and Wright, P. E. (2000) Amide proton exchange rates for sperm whale myoglobin obtained from ^{15}N-^{1}H NMR spectra. *Protein Sci. 9*, 186–193.
(32) Eliezer, D., Chung, J., Dyson, J. H., and Wright, P. E. (2000) Native and non-native secondary structure and dynamics in the pH 4 intermediate of apomyoglobin. *Biochemistry 39*, 2894–2901.
(33) Yao, J., Chung, J., Eliezer, D., Wright, P. E., and Dyson, J. H. (2001) NMR structural and dynamic characterization of the acid-unfolded state of apomyoglobin provides insights into the early events in protein folding. *Biochemistry 40*, 3561–3571.
(34) Lietzow, M. A., Jamin, M., Dyson., J. H., and Wright, P. E. (2002) Mapping long-range contacts in a highly unfolded protein. *J. Mol. Biol. 322*, 655–662.
(35) Griko, Y. V., Privalov, P. L., Venyaminov, S. Y., and Kutyshenko, V. P. (1988) Thermodynamic study of the apomyoglobin structure. *J. Mol. Biol. 202*, 127–138.
(36) Eliezer, D., Jennigs, P. A., Wright, P. E., Doniash, S., Hodgson, K. O., and Tsuruta, H. (1995) The radius of gyration of an apomyoglobin folding intermediate. *Science 270*, 548–488.
(37) Wang, F., and Tang., X. (1996) Conformational heterogeneity and stability of apomyoglobin studies by hydrogen/deuterium exchange and electrospray ionization mass spectrometry. *Biochemistry 35*, 4069–4078.
(38) Jennings, P. A., Stone, M. J., and Wright, P. E. (1995) Overexpression of myoglobin and assignments of it amide, C^{α} and C^{β} resonances. *J. Biomol. NMR. 6*, 271–276.
(39) Springer, B., and Sligar, S. G. (1987) High-level expression of sperm whale myoglobin in *Escherichia coli*. *Proc. Natl. Acad. Sci. U.S.A. 84*, 8961–8965.
(40) Altenbach, C., Kusnetzow, A. K., Ernst, O. P., Hofmann, K. P., and Hubbell, W. L. (2008) High-resolution distance mapping in rhodopsin reveals the pattern of helix movement due to activation. *Proc. Natl. Acad. Sci. U.S.A. 105*, 7439–7444.
(41) Jeschke, G. (2006) DeerAnalysis2006: A comprehensive software package for analyzing pulse ELDOR. *Appl. Magn. Reson. 191*, 473–498.
(42) Fraczkiewicz, R., and Braun, W. (1998) Exact and efficient analytical calculation of the accessible surface areas and their gradients for macromolecules. *J. Comput. Chem. 19*, 319–333.
(43) Langen, R., Oh, K. J., Cascio, D., and Hubbell, W. L. (2000) Crystal structures of spin labeled T4 lysozyme mutants: Implications for the interpretation of EPR spectra in terms of structure. *Biochemistry 39*, 8396–8405.
(44) Kroncke, B. M., Horanyi, P. S., and Columbus, L. (2010) Structural origins of nitroxide side chain dynamics on membrane protein α-helical sites. *Biochemistry 49*, 10045–10060.
(45) Hargrove, M. S., Barrick, D., and Olson, J. S. (1996) The association rate constant for heme binding to globin is independent of protein structure. *Biochemistry 35*, 11293–11299.
(46) Mchaourab, H. S., Lietzow, M. A., Hideg, K., and Hubbell, W. L. (1996) Motion of spin-labeled side chains in T4 lysozyme. Correlation with protein structure and dynamics. *Biochemistry 35*, 7692–7704.
(47) Zhang, Z., Fleissner, M. R., Tipikin, D. S., Liang, Z., Moscicki, J. K., Earle, K. A., Hubbell, W. L., and Freed, J. H. (2010) Multifrequency electron spin resonance study of the dynamics of spin labeled T4 lysozyme. *J. Phys. Chem. B 114*, 5503–5521.
(48) Columbus, L. (2001) Investigating Backbone and Side Chain Dynamics of α-Helices in the Nanosecond Regime by Site-Directed Spin Labeling, Ph.D. Thesis, University of California, Los Angeles, CA.
(49) Fleissner, M. R. (2007) X-ray Structures of Nitroxide Side Chains in Proteins: A Basis for Interpreting Distance Measurements and Dynamic Studies by Electron Paramagnetic Resonance, Ph.D. Thesis, University of California, Los Angeles, CA.
(50) Warshaviak, D. T., Serbulea, L., Houk, K. N., and Hubbell, W. L. (2011) Conformational analysis of a nitroxide side chain in an α-helix with density functional theory. *J. Phys. Chem. B 115*, 397–405.
(51) Budil, D. E., Lee, S., Saxena, S., and Freed, J. H. (1996) Nonlinear-least-squares analysis of slow-motion EPR spectra in one and two dimensions using a modified Levenberg-Marquard algorithm. *J. Magn. Reson. Ser. A 120*, 155–189.
(52) Arakawa, T., and Timasheff, S. N. (1985) The stabilization of proteins by osmolytes. *Biophys. J. 47*, 411–414.
(53) Liu, Y., and Bolen, B. D. (1995) The peptide backbone plays a dominant role in protein stabilization by naturally occurring osmolytes. *Biochemistry 34*, 12884–12891.
(54) Flores, R. H., Cao, M. D., Kim, M., and Cafiso, D. S. (2010) Osmolytes modulate conformational exchange in solvent-exposed regions of membrane proteins. *Protein Sci. 19*, 269–278.
(55) Hughson, F. M., Wright, P. E., and Baldwin, R. L. (1990) Structural characterization of a partially folded apomyoglobin intermediate. *Science 249*, 1544–1548.
(56) Jennings, P. A., and Wright, P. E. (1993) Formation of a molten globule intermediate early in the kinetic folding pathway of apomyoglobin. *Science 262*, 892–896.
(57) Nishimura, C., Dyson, J. H., and Wright., P. E. (2002) The apomyoglobin folding pathway revisited: Structural heterogeneity in the kinetic burst phase intermediate. *J. Mol. Biol. 322*, 483–489.
(58) Armstrong, B. D., Choi, J., López, C., Wesener, D. A., Hubbell, W., Cavagnero, S., and Han, S. (2011) Site-specific hydration dynamics in the nonpolar core of a molten globule by dynamic nuclear polarization of water. *J. Am. Chem. Soc. 113*, 5987–5995.
(59) Qu, K. B., Vaughn, J. L., Sienkiewicz, A., Scholes, C. P., and Fetrow, J. S. (1997) Kinetics and motional dynamics of spin-labeled yeast Iso-1-cytochrome *c*: 1. Stopped-flow electron paramagnetic resonance as a probe for protein folding/unfolding of the C-terminal helix spin-labeled at cysteine 102. *Biochemistry 36*, 2884–2897.
(60) Langen, R., Cai, K., Altenbach, C., Khorana, H. G., and Hubbell, W. L. (1999) Structural features of the C-terminal domain of bovine rhodopsin: a site-directed spin-labeling study. *Biochemistry 38*, 7918–7924.
(61) Pannier, M., Veit, S., Godt, A., Jeschke., G., and Speiss, H. W. (2000) Dead-time free measurement of dipole-dipole interactions between electron spins. *J. Magn. Reson. 142*, 331–340.
(62) Jeshke, G. (2002) Distance measurements in the nanometer range by pulse EPR. *ChemPhysChem 3*, 927–932.

(63) Jeschke, G., and Polyhach, Y. (2007) Distance measurements on spin-labeled biomacromolecules by pulsed electron paramagnetic resonance. *Phys. Chem. Chem. Phys. 9*, 1895−1910.
(64) Bracken, C., Carr, P. A., Cavanagh, J., and Palmer, A. G. (1999) Temperature dependence of intramolecular dynamics of the basic leucine zipper of GCN4: implications for the entropy of association with DNA. *J. Mol. Biol. 285*, 2133−2146.
(65) Morin, B., Bourhis, J. M., and Longhi, S. (2006) Assessing induced folding of an *IDP* by SDSL EPR spectroscopy. *J. Phys. Chem. B 110*, 20596−20608.
(66) Belle, V., Rouger, S., Costanzo, S., Liquiere, E., Strancar, J., Guigliarelli, B., Fournel, A., and Longhi, S (2008) Mapping alpha-helical induced folding within the intrinsically disordered C-terminal domain of the measles virus nucleoprotein by site-directed spin-labeling EPR spectroscopy. *Proteins 73*, 973−988.
(67) Sezer, D., Freed, J. H., and Roux, B. (2008) Parametrization, molecular dynamics simulation, and calculation of electron spin resonance spectra of a nitroxide spin label on a polyalanine alpha-helix. *J. Phys. Chem. B. 112*, 5755−5767.
(68) Mittermaier, A., Kay, L. E., and Forman-Kay, J. D. (1999) Analysis of deuterium relaxation-derived methyl axis order parameter and correlation with local structure. *J. Biomol. NMR 13*, 181−185.
(69) Goodman, J. L., Pagel, M. D., and Stone, M. J. (2000) Relationship between protein structure and dynamics from a database of NMR-derived backbone order parameters. *J. Mol. Biol. 295*, 963−978.
(70) Zhang, F., and Brüshweiler, R. (2002) Contact model for the prediction of NMR N-H order parameter in globular proteins. *J. Am. Chem. Soc. 124*, 12654−12655.
(71) Huang, S. H., Shih, C. H., Lin, C. P., and Hwang, J. K. (2008) Prediction of NMR order parameters in proteins using weighted protein contact number. *Theor. Chem. Acc. 121*, 197−200.
(72) Halle, B. (2002) Flexibility and packing in proteins. *Proc. Natl. Acad. Sci. U.S.A. 99*, 1274−1279.
(73) Phillips, G. N. (1990) Comparison of the dynamics of myoglobin in different crystal forms. *Biophys. J. 57*, 381−383.
(74) Frauenfelder, H., Hartmann, H., Karplus, M., Kuntz, I. D., Kuriyan, J., Parak, F., Petsko, G. A., Ringe, D., Tilton, R. F., Connolly, M. L., and Max, N. (1987) Thermal expansion of a protein. *Biochemistry 26*, 254−261.
(75) Fadel, A. R., Jin, D. Q., Montelione, G. T., and Levy, E. M. (1995) Crankshaft motions of the polypeptide backbone in molecular dynamics simulations of human type-α transforming growth factor. *J. Biomol. NMR. 6*, 221−226.
(76) Phillips, S. E. V. (1980) Structure and refinement of oxymyoglobin at 1.5Å resolution. *J. Mol. Biol. 142*, 531−554.
(77) Kachalova, G. A., Popov, A. N., and Bartunik, H. D. (1999) A steric mechanism for inhibition of CO binding to heme proteins. *Science 284*, 473−476.
(78) Parsegian, V. A. (2006) Van der Waals Forces, *A Handbook for Biologists, Chemists, Engineers, and Physicists*, Cambridge University Press, New York.
(79) Hambly, D. M., and Gross, M. L. (2005) Laser flash photolysis of hydrogen peroxide to oxidize protein solvent accessible residues on the microsecond timescale. *J. Am. Soc. Mass. Spectrom. 16*, 2057−2063.
(80) Van Eps, N., Anderson, L. L., Kisselev, O. G., Baranski, T. J., Hubbell, W. L., and Marshall, G. R. (2010) Electron paramagnetic resonance studies of functionally active, nitroxide spin-labeled peptide analogues of the C-terminus of a G-protein α subunit. *Biochemistry 49*, 6877−6886.